Materials Research Proceedings 41 (2024) 210-215 https://doi.org/10.21741/9781644903131-23

Impact of heat treatment cycles on work hardening characteristics in selective laser melted Ti6Al4V ELI alloy

SUKRE Mahendra[1,2,a] and MEENA Anil[1,b*]

[1]Department of Mechanical Engineering, Indian Institute of Technology Madras, Chennai-600036, India
[2]Shri Guru Gobind Singhji Institute of Engineering and Technology, Nanded, Maharashtra, India

[a]mdsukre@sggs.ac.in, [b]anilm@iitm.ac.in

Keywords: Selective Laser Melting (SLM), Heat Treatment, Ti6Al4V (ELI), Work Hardening Behaviour

Abstract. The present study investigates the influence of heat treatment cycles on the work hardening behaviour of a selective laser-melted (SLM) Ti6Al4V ELI alloy. To modify the microstructure and assess its impact on work hardening behaviour, the SLM Ti6Al4V ELI alloy is subjected to a series of heat treatment cycles, including solution treatment, quenching, and ageing. The microstructural evolution is characterized using scanning electron microscopy (SEM) and X-ray diffraction (XRD). Tensile tests are conducted to investigate the work hardening behaviour, including yield strength, ultimate tensile strength, and strain hardening. The findings show that heat treatment cycles have a significant impact on the microstructure and work hardening behavior of the SLM Ti6Al4V ELI alloy. Solution treatment and quenching produce a refined α' martensitic structure by homogenizing the microstructure and dissolving the secondary phases. Subsequent ageing treatments induce the precipitation of secondary phases, such as α and β phases, within the α' martensite matrix.

Introduction

Titanium alloys are widely used in the aerospace, automotive, medical, and chemical industries because of their important properties, which include biocompatibility, excellent corrosion resistance, and high specific strength [1,2]. Titanium alloys are primarily used in the aerospace industry to reduce weight and fuel consumption. Ti6Al4V is the most commonly used titanium alloy in industry [3]. However, due to the costs of mineral extraction, refinement, and manufacturing, product costs are high. As with mineral extraction costs, refinement costs are unavoidable [4]. As a result, industries require cost-effective solutions to reduce titanium alloy product manufacturing costs by reducing machining costs. Additive manufacturing (AM) is a low-cost solution for industries that reduces material costs (due to the reuse of powder) and tooling costs. It can also create complex components with the desired mechanical properties [5].

The most common AM process for metal AM manufacturing is selective laser melting (SLM). Manufacturing defects such as lack of fusion and porosity [6] can occur in titanium alloy SLM processes, affecting the mechanical performance of the additively manufactured component by increasing the stress concentration in the material. However, the material's microstructure plays an important role in determining its mechanical properties. The microstructure is determined by process parameters (laser power, layer thickness, and speed), design parameters (shape and size), and machine parameters (heated bed temperature) [5,7]. The direction of heat transfer causes columnar grains to form during selective laser melting. Because the crystals' growth direction is aligned with the maximum temperature gradient, the grains grow toward the molten pool in the z-direction. Furthermore, rapid cooling rates in small molten pools result in the formation of a metastable martensitic microstructure [8,9]. A fine microstructure can increase component

strength while decreasing ductility and work hardening. The main challenge in the AM component is balancing the material's strength, ductility, and work hardening. The heat treatment technique can help improve the mechanical properties and performance of Ti6Al4V components. However, traditional heat treatment is ineffective in achieving the desired mechanical properties [10]. Previous research suggests that work-hardening occurs due to kinematic hardening caused by the mechanical contrast between the α and α′ phases in electron beam-melted Ti6Al4V [11]. Stress-relieved samples exhibited a fine acicular martensitic α′ phase due to rapid solidification caused by LPBF [12].

This study investigated the impact of heat treatment on the microstructure and work hardening behavior of SLMed Ti6Al4V ELI below the trans temperature. Two heat treatment cycles were used: HT-730 and HT-940-540. Tensile tests were performed on both as-received and heat-treated samples to determine the material's work-hardening parameter. The study proposed a straightforward method for linking heat treatment, work hardening, and SLMed Ti6Al4V ELI alloys.

Experimental procedure

All samples were created using the SLM machine in the presence of argon inert gas. The feedstock material used was Ti6Al4V ELI powders. The powder size ranged from 10 μm to 60 μm, with a 31 μm average. For sample production, the default manufacturing parameters were used. The rectangular samples were created vertically along the Z-axis. Three samples were made for each process condition. Following the printing process, the samples were stress-relieved under specific conditions: 800°C for 2 hours, followed by furnace cooling to 300°C and air cooling to room temperature. Using wire-EDM, the samples were cut from build plates. As shown in Table 1, heat treatments were used to modify the microstructure of stress-relieved samples. Both stress relief and heat treatment took place in an inert gas environment. Micro tensile testing was performed on sub-sized rectangular samples with a gauge length of 6 mm, as defined by ASTM E8/E8M. A micro-tensile testing system with a load cell capacity of 2 kN was used, with a constant strain rate of 0.001 s^{-1} applied during testing. Additionally, rectangular samples measuring 5 × 10 × 10 mm^3 were produced for metallography. Standard metallographic sample preparation procedures, such as sectioning, grinding, and polishing, were used. Kroll's reagent was used as an etchant. The microstructure was studied using a digital microscope (Olympus GX53 Inverted) and a scanning electron microscope (INSPECT F50 FE-SEM). The Bruker D8 Discover powder XRD machine was used for the X-ray diffraction (XRD) analysis.

Table 1: Heat treatment cycle performed on the SLM Ti6Al4V ELI

Terminology	Heat treatment condition
As received (AR)	Stress relieved
HT-730	Heating at 730 ºC for 2h and AC*
HT-940-550	Heating at 940 ºC for 1h and WQ* + Aging at 550 ºC for 4h and AC*

* AC- Air cooling, WQ- Water quenching

Results and Discussions

The optical microscopic image of the AR and heat-treated sample, shown in Fig. 1, depicts the material's microstructure. However, as a proper process section, 3D printing parameters significantly reduce pore amount and size [13]. As shown in Fig. 1, the sample has an equiaxed microstructure. The columnar grain will be visible in the build direction's longitudinal section. All microstructural features are difficult to detect on an optical microscopic image. The grain boundaries visible in the heat-treated samples, on the other hand, are indicated with dashed lines in Fig. 1 (a), (b), and (c). The acicular microstructure of the AR samples allows for the detection

of grain boundaries. SEM and XRD analyses have been performed to extract detailed microstructure information, and phase identification. The phase and grain size are consistent in all directions. As a result, SEM and XRD tests are performed on the transverse section of the built direction in all samples.

Figure 2 depicts the XRD pattern of AR and heat-treated samples. The pattern of AR samples shows a high amount of martensitic phase and a very small amount of peak, which corresponds to the microstructure feature of the SEM of AR samples in Fig. 2. Some studies indicate the absence of the β peak in the as-built sample. This distinction was caused by the stress-relieving step that followed the printing process. The martensitic α' phase decomposed into α+β phases during the HT 730 heat treatment process, as indicated by the β peaks. However, the HT-940-550 specimen showed minimal presence of the β phase.

Table 2 compares the tensile properties of different Ti6Al4V (ELI) samples, including SLMed, AR, and heat-treated samples. The AR sample has high ultimate tensile strength (UTS) and yield strength (YS), but low elongation (EL) due to the presence of fine acicular α' martensite, a well-studied feature. However, the HT-730 heat treatment significantly improves elongation. This improvement could be attributed to an increase in the average width of the α lathe, as shown in Fig. 3 (b). The presence of transformed β grains also helps to increase ductility.

HT-730 specimens have slightly lower ultimate tensile and yield strengths (UTS) due to larger α laths and β intercrystalline grains. Although the HT-940-550 specimen has coarser α laths, which improve UTS and YS, there is a noticeable decrease in ductility. As shown in Fig. 3 (c), this is due to the presence of extremely fine and dispersed α+β grains interspersed among the coarse α laths. These grains impede lath plastic deformation, resulting in relatively high UTS and YS values. As a result, the HT-940-540 treatment offers a balanced combination of high tensile strength and ductility, making it an ideal solution for heat treatment in SLMed Ti6Al4V ELI.

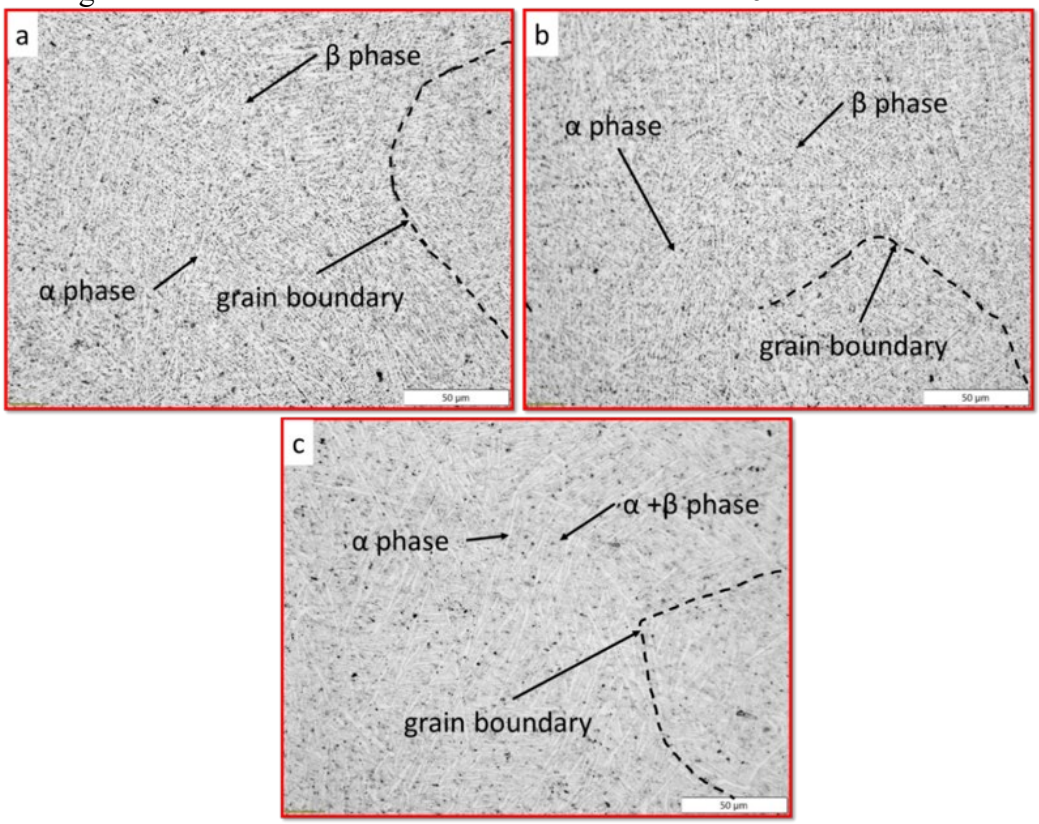

Fig. 1: Microstructure image of Ti6Al4V ELI using optical microscopic image of (a) as received sample (b) HT-730 (c) HT-940-550 (α phase indicated by the light shade and β phase indicated by dark shade).

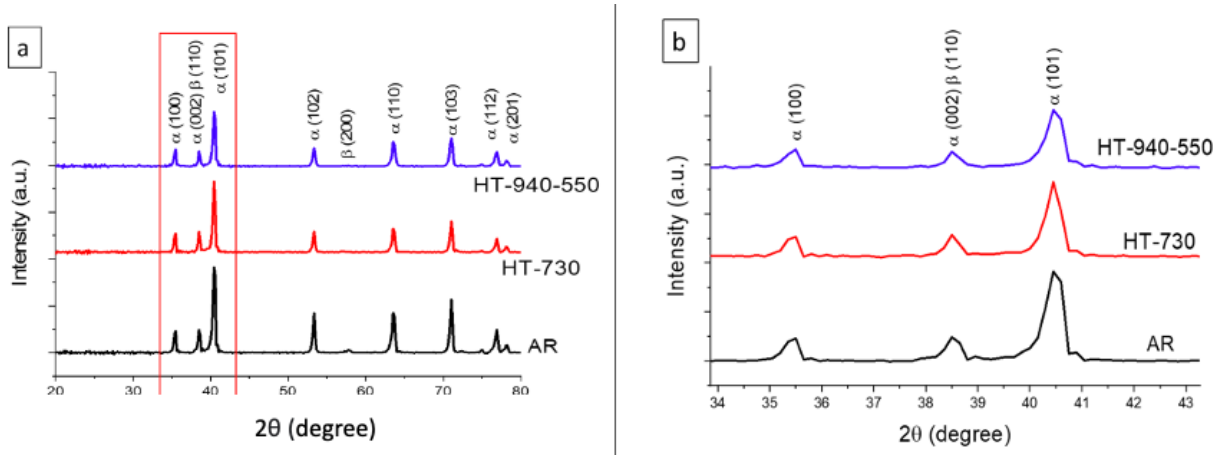

Fig. 2: X-ray diffraction of (a) as received and heat-treated samples shows the different phases (b) magnified view of X-ray diffraction.

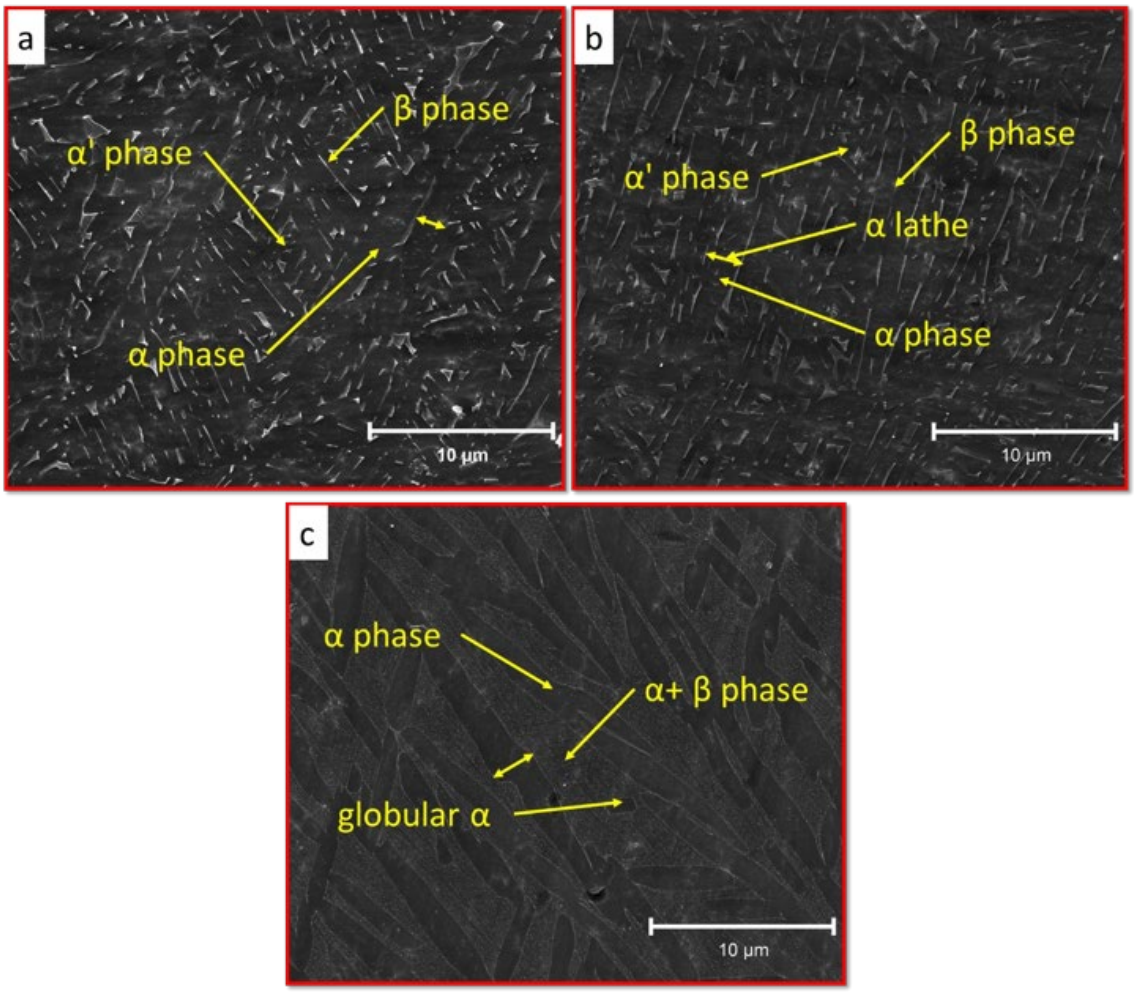

Fig. 3: Microstructure image of Ti6Al4V ELI using scanning electron microscopy image of (a) as received sample (b) HT-730 (c) HT-940-550 (α phase indicated by the dark shade and β phase indicated by light shade).

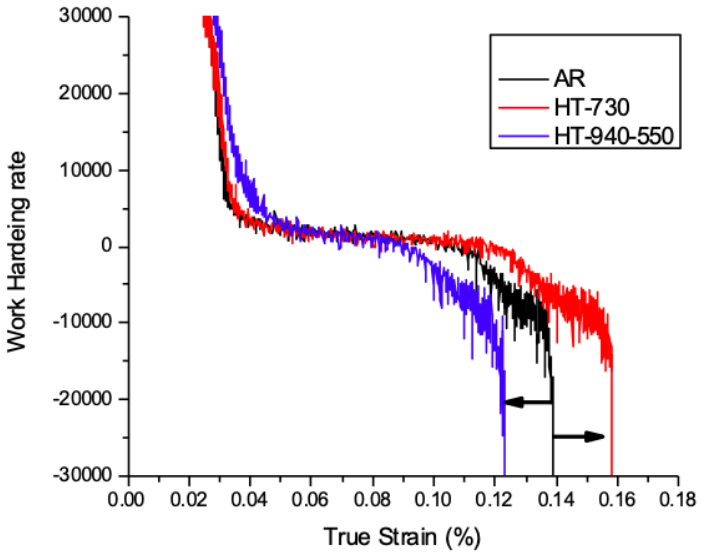

Fig. 4: Work hardening rate plotted as a function of true strain.

Table 2: Mechanical properties of SLM Ti6Al4V ELI with AR and heat-treated samples

	YS (MPa)	UTS (MPa)	% Elongation	Hardening capacity
As received (AR)	1026 ± 20	1110 ± 3	14	0.082
HT-730	1016 ± 6	1086 ± 5	16	0.069
HT-940-550	1091 ± 12	1197 ± 11	13	0.098

The rate at which the flow stress changes with strain is referred to as the work hardening rate. The work hardening rate in AR and heat-treated conditions is calculated in this study. The mathematical equation for the work hardening rate is as follows:

$$\frac{d\sigma}{d\varepsilon} = \frac{\sigma_{i+1}-\sigma_i}{\varepsilon_{i+1}-\varepsilon_i} \quad (1)$$

The work hardening rate is depicted in Fig. 4 by taking the derivative of the tensile true-stress-true-strain curve under heat-treated conditions using the formula shown in eq. (1). All of the samples studied show a consistent pattern of work hardening rate. The work hardening rate initially decreased significantly before stabilizing at a constant value under quasi-static conditions. A more gradual shift in the work hardening rate, as shown in Fig. 4, is advantageous in achieving an improved balance between the material's ductility and strength. Furthermore, a decrease in the work hardening rate indicates a decrease in the material's work hardening capacity. The work hardening rate curve is divided into three stages: a strong stage, a stable stage, and a weak stage. The hardening rate in the HT-940-550 condition is higher than in the AR and HT-730 conditions, which can be attributed to finely dispersed α particles in the β phase. The work hardening rate is closely related to the retained α' martensite volume fraction of the material. There is a linear relationship between yield strength and work hardening rate, as well as an inverse relationship with material ductility.

Conclusions

The AR has an average acicular α' martensitic structure, which improves the YS and UTS of the material. This acicular α' martensite decreased after heat treatment. The average width of the α lathe of Ti6Al4V ELI is critical in determining the material's work-hardening capacity. Because

of the coarsening of laths, HT-730 treatments can significantly improve the ductility of SLMed Ti6Al4V ELI, resulting in a decrease in the material's hardening capability. Because of the presence of α particles inside the β phase, HT-940-550 has the highest UTS and YS when compared to other heat treatment cycle. The work hardening rate of Ti6Al4V ELI decreased significantly as true strain increased. Heat treatment has a significant impact on the work hardening rate, with HT-940-550 exhibiting the highest work hardening rate.

References

[1] Y. Okazaki and A. Ishino, Microstructures and Mechanical Properties of Laser-Sintered Commercially Pure Ti and Ti-6Al-4V Alloy for Dental Applications, Materials 13 (2020) 1-18. https://doi.org/10.3390/ma13030609

[2] J. Lu, H. Lu, X. Xu, J. Yao, J. Cai, and K. Luo, *Int J Mach Tools Manuf* 148 (2020) 103475. https://doi.org/10.1016/j.ijmachtools.2019.103475

[3] B. Dutta, F.H. Froes: *Additive Manufacturing of Titanium Alloys : State of the Art, Challenges and Opportunities*, vol. 1, 1st edn., Elsevier, Oxford, 2016.

[4] F. Froes, M.N. Gungor, M. Ashraf Imam, Cost-affordable titanium: the component fabrication perspective, JOM 59 (2007) 28-31. https://doi.org/10.1007/s11837-007-0074-8

[5] J. Zhang, B. Song, Q. Wei, D. Bourell, Y. Shi, A review of selective laser melting of aluminum alloys: Processing, microstructure, property and developing trends, *Journal of Materials Science & Technology* 35.2 (2019) 270-284. https://doi.org/10.1016/j.jmst.2018.09.004

[6] S. Cao, Z. Chen, C.V.S. Lim, K. Yang, Q. Jia, T. Jarvis, D. Tomus, X. Wu, Defect, microstructure, and mechanical property of Ti-6Al-4V alloy fabricated by high-power selective laser melting, *JOM* 69.12 (2017) 2684-2692. https://doi.org/10.1007/s11837-017-2581-6

[7] Ó. Teixeira, F.J.G. Silva, E. Atzeni, Residual stresses and heat treatments of Inconel 718 parts manufactured via metal laser beam powder bed fusion: an overview, *The International Journal of Advanced Manufacturing Technology* 113.11-12 (2021) 3139-3162. https://doi.org/10.1007/s00170-021-06835-8

[8] D. Chen, P. Wang, R. Pan, C. Zha, J. Fan, D. Liang, Y. Zhao, Characteristics of metal specimens formed by selective laser melting: a state-of-the-art review, *Journal of Materials Engineering and Performance* 30 (2021) 7073-7100. https://doi.org/10.1007/s11665-020-05323-6

[9] N.T. Aboulkhair, M. Simonelli, L. Parry, I. Ashcroft, C. Tuck, R. Hague, 3D printing of Aluminium alloys: Additive Manufacturing of Aluminium alloys using selective laser melting, *Progress in materials science* 106 (2019) 100578. https://doi.org/10.1016/j.pmatsci.2019.100578

[10] B. Vrancken, L. Thijs, J.P. Kruth, J. Van Humbeeck, Heat treatment of Ti6Al4V produced by Selective Laser Melting: Microstructure and mechanical properties, *Journal of Alloys and Compounds* 541 (2012) 177-185. https://doi.org/10.1016/j.jallcom.2012.07.022

[11] C. de Formanoir, A. Brulard, S. Vivès, G. Martin, F. Prima, S. Michotte, E. Rivière, A. Dolimont, and S. Godet, A strategy to improve the work-hardening behavior of Ti–6Al–4V parts produced by additive manufacturing, *Materials Research Letters* 5.3 (2017) 201-208. https://doi.org/10.1080/21663831.2016.1245681

[12] A. Mahmud, T. Huynh, L. Zhou, H. Hyer, A. Mehta, D.D. Imholte, N.E. Woolstenhulme, D.M. Wachs, and Y. Sohn, Mechanical behavior assessment of Ti-6Al-4V ELI alloy produced by laser powder bed fusion, *Metals* 11.11 (2021) 1671. https://doi.org/10.3390/met11111671

[13] H. Yu, F. Li, Z. Wang, and X. Zeng, Fatigue performances of selective laser melted Ti-6Al-4V alloy: Influence of surface finishing, hot isostatic pressing and heat treatments, *International Journal of Fatigue* 120 (2019) 175-183. https://doi.org/10.1016/j.ijfatigue.2018.11.019

[14] Rodney. Boyer, Gerhard. Welsch, and E.W. Collings: *Materials Properties Handbook : Titanium Alloys*, ASM International, 1994.